SUPPLEMENTARY DATA

# Action at Hooked or Twisted-Hooked DNA Juxtapositions Rationalizes Unlinking Preference of Type-2 Topoisomerases

**Zhirong LIU**,[1,2*] **Lynn ZECHIEDRICH**[3] and **Hue Sun CHAN**[2,4*]

[1] College of Chemistry and Molecular Engineering,
Center for Theoretical Biology, and Beijing National Laboratory for Molecular Sciences,
Peking University, Beijing 100871, China[†]

[2] Departments of Biochemistry and of Molecular Genetics, University of Toronto,
Toronto, Ontario M5S 1A8, Canada

[3] Department of Molecular Virology and Microbiology, Verna and Marrs McLean
Department of Biochemistry and Molecular Biology, and Department of Pharmacology,
Baylor College of Medicine, Houston, Texas 77030, U.S.A.

[4] Department of Physics, University of Toronto, Toronto, Ontario M5S 1A7, Canada

---

∗ Corresponding authors.
E-mail addresses: liuzhirong@pku.edu.cn; chan@arrhenius.med.toronto.edu
[†] Present address of Z.L.

# Appendix

## CONJUGATE JUXTAPOSITIONS AND WRITHE MAPS OF CIRCLES WITH A PREFORMED JUXTAPOSITION

### Rationale and consequences of $j^*$-symmetrization

We provide further technical details in this Appendix about the symmetrized virtual segment passage procedure introduced in Materials and Methods. The notation here is identical to that in the main text. Figure S1 provides data for the hooked and free juxtapositions in our model and compare them with the ideal case. In the hypothetical ideal case with zero contact distance ($d = 0$), the population of conformations constrained by any given preformed juxtaposition should be equal to that constrained by its conjugate juxtaposition, i.e., $(P_j)_{\rm eq} = (P_{j^*})_{\rm eq}$, even though their topological distributions can be different. Fig. S1(a) shows that the self-avoiding lattice chain model is far from ideal in this respect. There are always more lattice conformations with a hooked juxtaposition than with a free juxtaposition; the difference increases for smaller circles. A part of this trend may be physically plausible for real DNA because different juxtaposition geometries entail different excluded volume constraints. But the large $(P_j)_{\rm eq}/(P_{j^*})_{\rm eq}$ population ratios in Fig. S1(a) for small to intermediate-sized circles ($n \lesssim 100$) would seem unreasonably large for a real DNA juxtaposition geometry acted upon by type-2 topoisomerases.

In the same vein, Fig. S1(b) compares the forward flux from one knotted or unknotted state to another state via the hooked juxtaposition against the reverse flux via the conjugate free juxtaposition. Ideally, for juxtapositions with zero contact distance, such forward and reverse fluxes should be equal. However, in the lattice model, Fig. S1(b) shows that forward and reverse fluxes are far from equal for $n \lesssim 100$, even though the discrepancy diminishes for larger $n$. In particular, the plot exhibits a noticeably higher U$\leftrightarrow$K curve and a markedly lower K$\leftrightarrow$U curve. These features demonstrate that in the absence of $j^*$-symmetrization, there is a bias toward creating knotted conformations by segment passage, as we have argued in the main text. Based on this understanding, the link and knot reduction factors we determined previously [1,2] may be viewed as underestimates, with the recognition that disentangling powers can be higher when geometrically more realistic $j^*$-symmetrized operations are used. The ratios for the quantities plotted in Fig. S1 would all effectively become the ideal value of unity under $j^*$-symmetrization.

Using the mutually conjugating hooked and free juxtapositions again as an example, Fig. S2 shows how the virtual segment passage process effectively creates a large number of additional virtual conformations, as noted in the main text, and how this model feature depends on chain length $n$. The number of virtual conformations created by virtual segment passage is equal to the flux of the process. For idealized juxtapositions with zero contact distance, the flux/population ratio should equal unity. For self-avoiding simple cubic lattice circles, however, Fig. S2 shows that, for $n \lesssim 100$, the flux from the unknotted state through a juxtaposition is always larger than the number of conformations that have the conjugate juxtaposition [flux/population ratio $> 1$ for U$\rightarrow$K in both (a) and (b), ratio $> 1$ for U$\rightarrow$U as well in (a)]. This effect decreases with increasing chain length but increases sharply for very small $n$. Here, the effect is most prominent for unknotted conformations that undergo virtual segment passages at a free juxtaposition to become knotted conformations. In this case, even for the largest lattice circle studied ($n = 500$), the flux is almost five times that of the number of knotted conformations with a hooked juxtaposition [Fig. S2(b)], demonstrating once again that the virtual segment passage operation [1, 2] is biased in favor of creating knotted conformations.

All in all, Figs. S1 and S2 underscore the extent to which virtual segment passage beget a large number of virtual conformations, conformations that were not eligible for segment passage in our original formulation [1, 2]. As seen above, the magnitude of this imbalance in the model can be large and would likely lead to some limitations in modeling type-2 topoisomerase actions. Our $j^*$-symmetrization mitigates this imbalance by allowing virtual conformations to also undergo (reverse) virtual segment passages. It is important to emphasize, however, that the possibility of such limitations does not negate our previous positive assessment [1–3] of the hooked juxtaposition hypothesis [4]. The reason is that these imbalances tend to result in an underestimation, rather than an overestimation, of the ability of our model segment passage to disentangle. This point will be demonstrated explicitly below.

With the above considerations in mind, Fig. S3 compares the model link (catenane) and knot reduction factors determined using the original (not $j^*$-symmetrized) virtual segment passage procedure in refs. [1–3] against those computed using the present $j^*$-symmetrized procedure. Consistent with expectation, Fig. S3(a) and Fig. 3(b) show that the new link and knot reduction factors with $j^*$-symmmetrization (blue data points) are substantially higher (meaning a higher power to disentangle) than those without $j^*$-symmetrization (red data points). For instance, for the hooked juxtaposition (I), the link

reduction factor $R_{\rm L}$ for the $n = 100$ circles in Fig. S3 increases from $R_{\rm L} \approx 10$ with no $j^*$-symmetrization to $R_{\rm L} \approx 16$ with $j^*$-symmetrization. The corresponding increase of the knot reduction factor from $R_{\rm K} \approx 46$ (ref. [2]) to $R_{\rm K} \approx 225$ is even more pronounced. Interestingly, Fig. S3(b) shows that the juxtaposition that has the highest knot reduction factor with $j^*$-symmetrization is the twisted-hooked juxtaposition (V) with hookedness $H = 1$ ($R_{\rm K} \approx 245$) rather than the hooked juxtaposition (I) with $H = 2$. The correlation between the logarithmic link reduction factor and logarithmic knot reduction factors with $H$ is also significantly higher under $j^*$-symmetrization (see $r$ values in caption for Fig. S3). Finally, Fig. S3(c) and Fig. S3(d) examine the relationship between the link and knot reduction factors determined with and without $j^*$-symmetrization. The overall correlation is reasonable but there is also considerable scatter. Notably, the correlation is better among those juxtapositions that disentangle ($\log R_{\rm L} > 0$, $\log R_{\rm K} > 0$) in the $j^*$-symmetrized scheme.

**Probing the effects of a preformed juxtaposition by shifted writhe maps**

Next, we follow the analysis of the writhe profile $Wr(i)$ in the main text to develop a more panoramic view of how geometrical constrains imposed by the presence of a juxtaposition affects the writhe of a small circle differently from that of a large circle. Here we examine the effects of a juxtaposition on the writhe map $Wr(i, j)$ in eq. (27) in the main text. We refer to the separation along the chain sequence between the two center beads of the juxtaposition as the order of the juxtaposition, and denote it by $k$. We further define $k$ to be the shorter of the separations (if they are different) along the two opposite contour directions such that $0 < k \leq n/2$. For circles configured on simple cubic lattices, $k$ is an odd number and $k \geq 5$. A preformed juxtaposition can exist in different orders, i.e., at multiple $k$ values. For a given preformed juxtaposition, we use $Wr(k|i, j)$ to denote the conditional writhe map subject to the constraint of an order $k$ juxtaposition. The construction of $Wr(k|i, j)$ is similar in spirit to the conditional contact maps used to study protein conformations [5, 6].

To assess the overall effect of a preformed juxtaposition irrespective of its location along the chain, it is useful to construct a shifted writhe map, as follows, in which juxtapositions of all orders are placed at the same spot. Beginning with the center beads of the juxtaposition at $i = i_0$ and at $j = j_0 = i_0 + k$, we shift label $i$ so that the first center bead is now at $i = n/2$. This entails redefining $i \rightarrow [(i - i_0 + 3n/2) \bmod n]$. We then make a shift on label $j$ to a new label $s$, a shift that depends on $k$ and is, in general,

different from the shift on $i$, so that the second center bead is now at $j \to s = n/2$. This requires $s = [(j - i_0 - k + 3n/2) \bmod n]$. These operations move the order-$k$ juxtaposition initially represented at $(i_0, j_0)$ on the $Wr(k|i, j)$, with $i_0 < j_0$, to a new position at the center of a map whose coordinates are the shifted label $i$ and label $s$. Now the bonds in the juxtaposition are at $i, s = n/2 - 2$, $n/2 - 1$, $n/2$, and $n/2 + 1$. We use $Wr^{(\mathrm{s})}(k|i, s)$ to denote the resulting shifted constrained writhe map. We then obtain the total shifted constrained writhe map $Wr^{(\mathrm{s})}(i, s)$ by summing contributions from all $k \leq n/2$, i.e., $Wr^{(\mathrm{s})}(i, s) = \sum_k Wr^{(\mathrm{s})}(k|i, s)$.

Figure S4 shows $Wr^{(\mathrm{s})}(i, s)$ for a single conformation as well as $\langle Wr^{(\mathrm{s})}(i, s) \rangle$ obtained by averaging $Wr^{(\mathrm{s})}(i, s)$ over an ensemble of conformations. In these shifted maps, the deep red (positive) spots at the center represent the contributions to $Wr$ from the cross products of the bonds within the preformed juxtaposition. The directions of the bonds outside the juxtaposition are allowed to varied. Their contributions to $Wr$ tend to average to small positive or negative values when conformational freedom is less restricted for large $n$ (pale coloring outside the center juxtaposition in Fig. S4(b) and (c)). In such cases, the contributions to $Wr$ arising from the preformed juxtaposition itself are dominant. Nonetheless, there is a clear difference between the hooked and the free juxtapositions. For larger circles with a hooked juxtaposition, contributions outside the juxtaposition region tend to be more constructive (more red along the diagonal with positive slope in the left panels in Fig. S4(b) and (c)) than the corresponding contribution for larger circles with a free juxtaposition (less red along the same diagonal in the right panels in Fig. S4(b) and (c)). This difference accounts for the higher $|Wr|$ values in large circles with a hooked juxtaposition than those with a free juxtaposition.

However, the situation for small circles is not the same because of tight connectivity. For a small circle with a hooked juxtaposition, there are substantial $Wr$ compensation, as we have already noted. This feature is underscored by the deep blue (negative) spots at, for example, $i, s = 6, 10$ in the map for the hooked juxtaposition in Fig. S4(a). In contrast, in the map for the free juxtaposition in Fig. S4(a), there are no deep blue spots. Instead, there are more pink and deep red spots outside the juxtaposition region in the center, echoing our finding in the main text that $Wr$ contributions from different parts of a small circle with a free juxtaposition tend to reinforce one another.

# References


[1] Liu, Z., Zechiedrich, E. L. & Chan, H. S. (2006). Inferring global topology from local juxtaposition geometry: interlinking polymer rings and ramifications for topoisomerase action. *Biophys. J.* **90**, 2344–2355.

[2] Liu, Z., Mann, J. K., Zechiedrich, E. L. & Chan, H. S. (2006). Topological information embodied in local juxtaposition geometry provides a statistical mechanical basis for unknotting by type-2 DNA topoisomerases. *J. Mol. Biol.* **361**, 268–285.

[3] Liu, Z., Deibler, R. W., Chan, H. S. & Zechiedrich, L. (2009). The why and how of DNA unlinking. *Nucl. Acids Res.* **37**, 661–671.

[4] Buck, G. R. & Zechiedrich, E. L. (2004). DNA disentangling by type-2 topoisomerases. *J. Mol. Biol.* **340**, 933–939.

[5] Chan, H. S. & Dill, K. A. (1990). The effects of internal constraints on the configurations of chain molecules. *J. Chem. Phys.* **92**, 3118–3135. Erratum: **107**, 10353 (1997).

[6] Chan, H. S. & Dill, K. A. (1990). Origins of structure in globular proteins. *Proc. Natl. Acad. Sci. USA* **87**, 6388–6392.

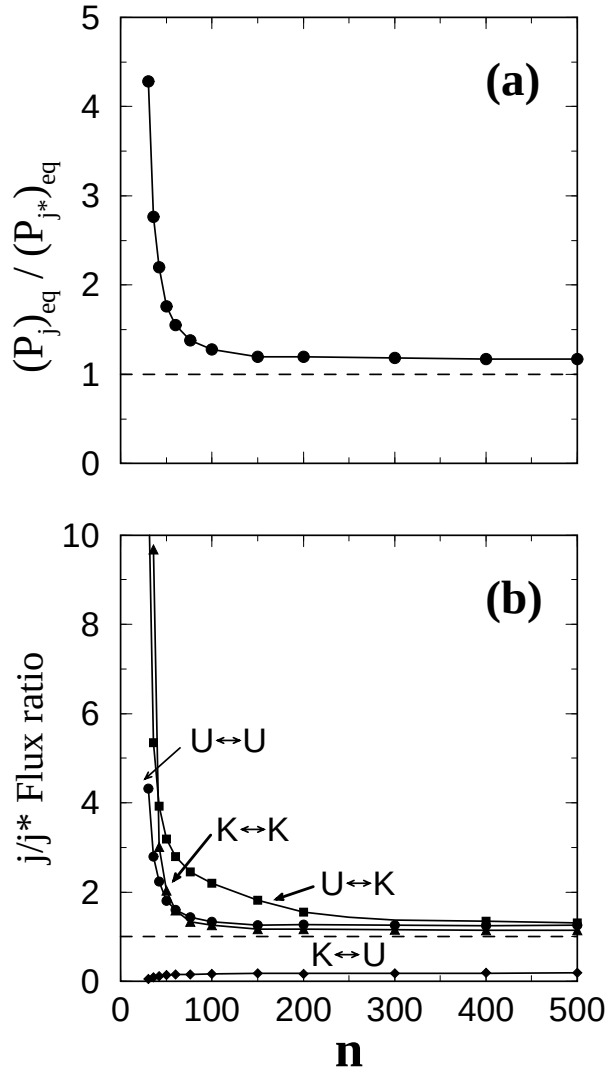


**Fig. S1.** Rationale for $j^*$-symmetrization in the lattice model. In this example, $j$ is the hooked juxtaposition and $j^*$ is the free juxtaposition. Shown as functions of chain length $n$ are (a) the number of conformations with a hooked juxtaposition divided by the number of conformations with a free juxtaposition, and (b) the number of possible transitions $N_j\mathcal{J}^{(j)}$ from a knotted (K) or unknotted (U) conformation to a K or U conformation via virtual segment passage at a hooked juxtaposition divided by the number of possible reverse transitions $N_{j^*}\mathcal{J}^{(j^*)}$ via virtual segment passage at a free juxtaposition. Curves in (b) labeled by U $\leftrightarrow$ U, K $\leftrightarrow$ K, U $\leftrightarrow$ K, and K $\leftrightarrow$ U are, respectively, $N_j\mathcal{J}^{(j)}_{\mathrm{U}\to\mathrm{U}}/N_{j^*}\mathcal{J}^{(j^*)}_{\mathrm{U}\to\mathrm{U}}$, $N_j\mathcal{J}^{(j)}_{\mathrm{K}\to\mathrm{K}}/N_{j^*}\mathcal{J}^{(j^*)}_{\mathrm{K}\to\mathrm{K}}$, $N_j\mathcal{J}^{(j)}_{\mathrm{U}\to\mathrm{K}}/N_{j^*}\mathcal{J}^{(j^*)}_{\mathrm{K}\to\mathrm{U}}$, and $N_j\mathcal{J}^{(j)}_{\mathrm{K}\to\mathrm{U}}/N_{j^*}\mathcal{J}^{(j^*)}_{\mathrm{U}\to\mathrm{K}}$. The ideal ratio of unity is marked by dashed lines in (a) and (b).

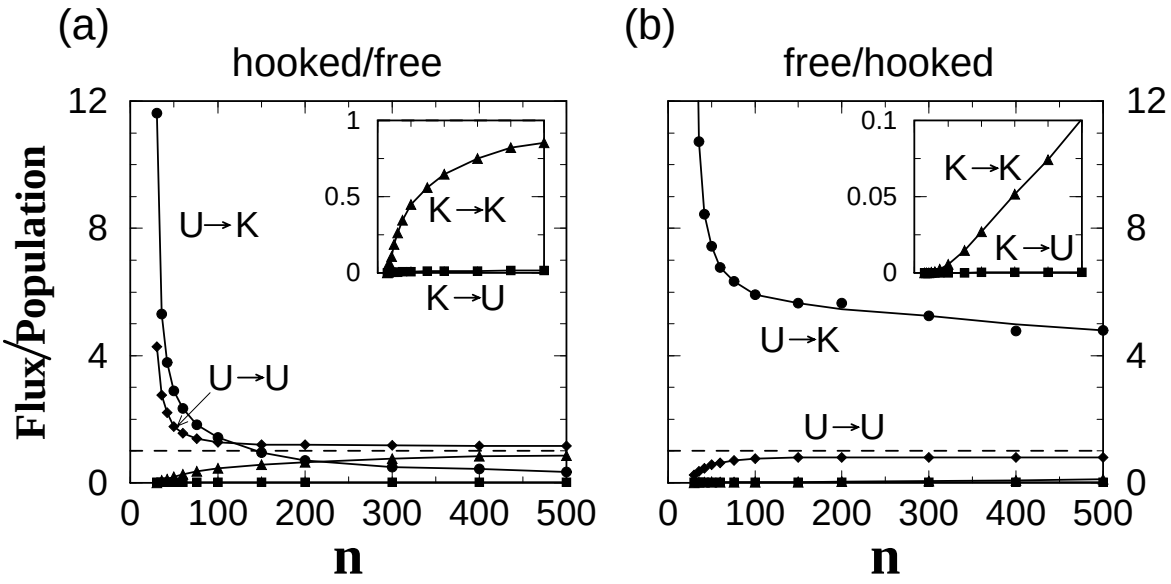


**Fig. S2.** Asymmetry between $j$ and $j^*$ and further rationale for $j^*$-symmetrization. (a) Each data point for a given chain length $n$ is the number of possible transitions from an initial conformation to a final conformation in a given knotted or unknotted state (K or U) via virtual segment passage at a hooked juxtaposition ($j$) divided by the number of conformations belonging to the given final state and containing a free juxtaposition ($j^*$). These ratios are given by $N_j \mathcal{J}^{(j)}_{\mathrm{U}\to\mathrm{U}}/P^{(j)}_{\mathrm{U}}$ (for U $\to$ U), $N_j \mathcal{J}^{(j)}_{\mathrm{K}\to\mathrm{K}}/P^{(j)}_{\mathrm{K}}$ (for K $\to$ K), $N_j \mathcal{J}^{(j)}_{\mathrm{U}\to\mathrm{K}}/P^{(j)}_{\mathrm{K}}$ (for U $\to$ K), and $N_j \mathcal{J}^{(j)}_{\mathrm{K}\to\mathrm{U}}/P^{(j)}_{\mathrm{U}}$ (for K $\to$ U). For clarity, the K $\to$ K and K $\to$ U curves below the dashed lines are also plotted in the inset. (b) Same as (a) except the roles of hooked and free juxtapositions are interchanged.

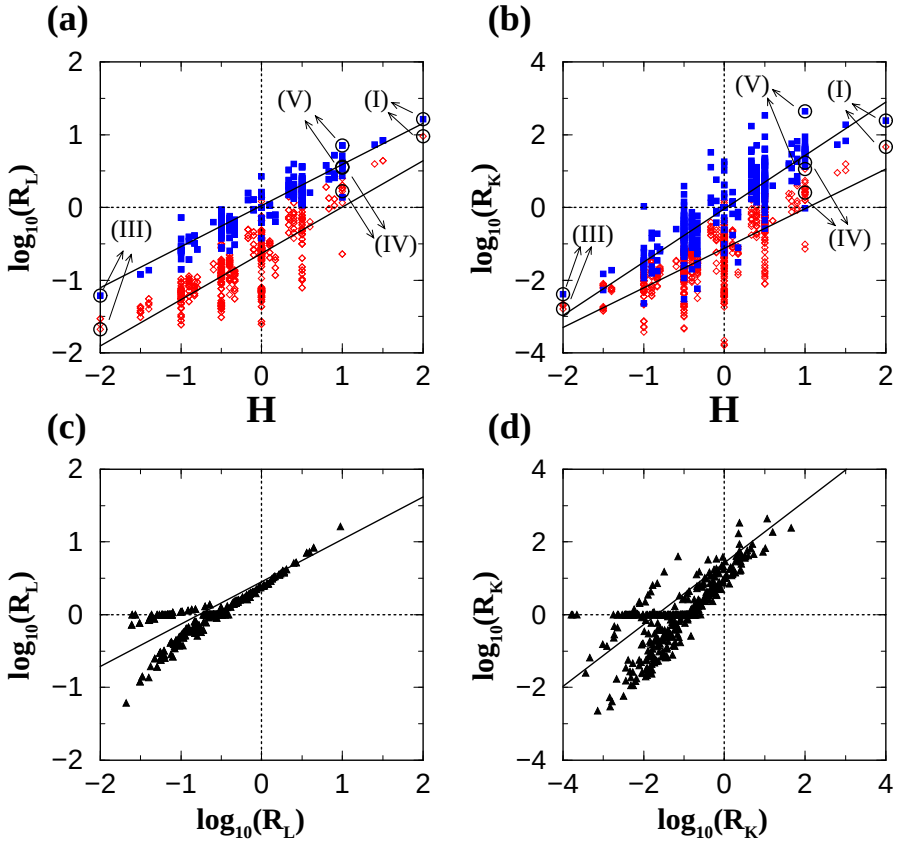


**Fig. S3.** Comparing link (catenane) and knot reduction factors with and without $j^*$-symmetrization. Scatter plots of (a) logarithmic link reduction factors and (b) logarithmic knot reduction factors with the hookedness parameter $H$ for $n = 100$ circles computed using $j^*$-symmetrization (blue squares) are compared against scatter plots of reduction factors determined previously [1–3] without $j^*$-symmetrization (red diamonds). Data points for the hooked (I), free (III), half-hooked (IV), and twisted-hooked (V) juxtapositions are labeled. The $r$ coefficients in (a) are 0.91 and 0.79, respectively, for $\log R_{\rm L}$ computed with and without $j^*$-symmetrization. The corresponding $r$ coefficients in (b) for $\log R_{\rm K}$ are 0.86 and 0.69. (c) Scatter plot of $\log R_{\rm L}$ computed using $j^*$-symmetrization (vertical scale) versus $\log R_{\rm L}$ computed without $j^*$-symmetrization (horizontal scale); $r = 0.83$. (d) Same as (c) but for $\log R_{\rm K}$, $r = 0.73$. All scatter plots in (a)–(d) are for the 425 juxtapositions that permit $j^*$-symmetrization except the red data points in (a) and (b) are for 680 juxtapositions, as for the bottom right panel of Fig. 7 in ref. [2]. Straight lines are least-square fits.

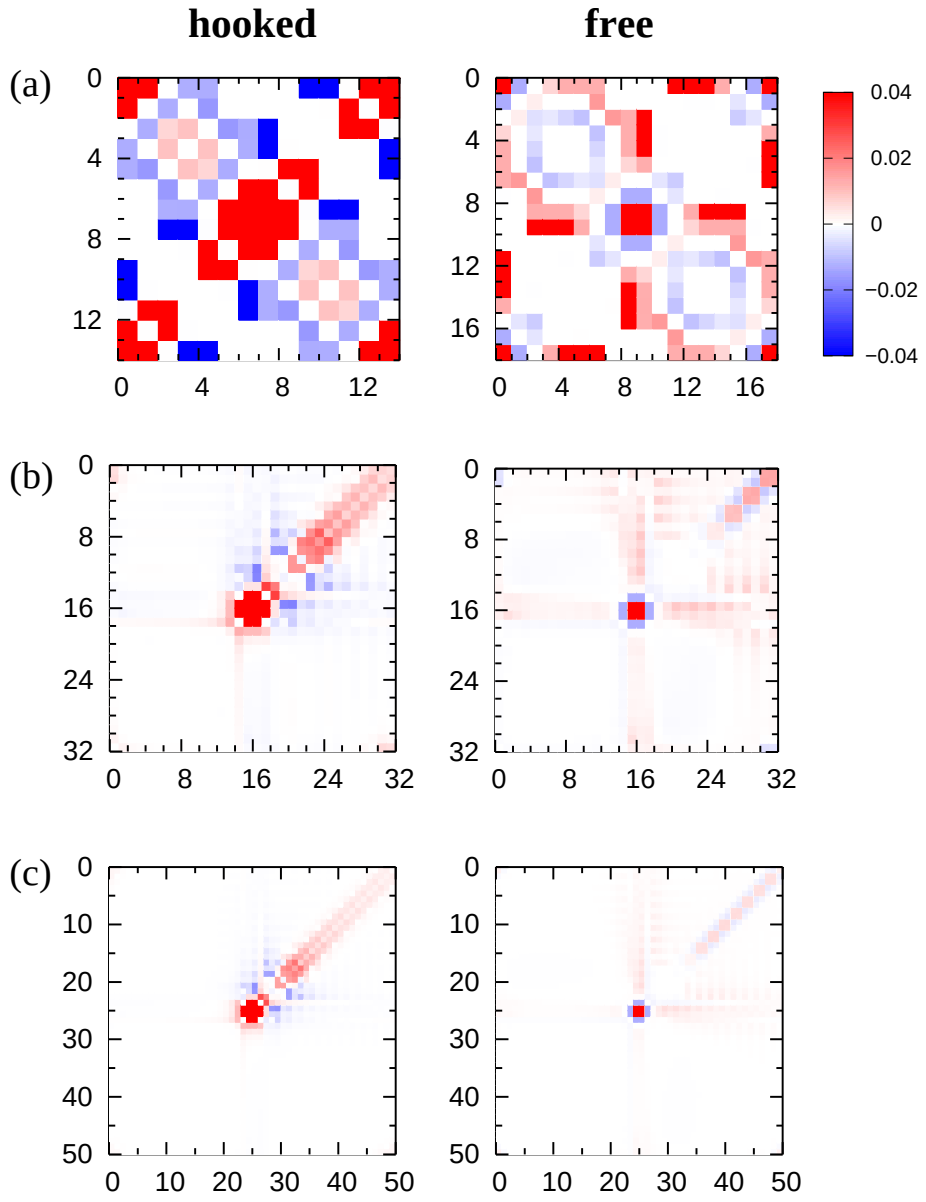


**Fig. S4.** Chain-length dependence of writhe maps with preformed juxtapositions. Shown here are shifted constrained $Wr^{(s)}(i,s)$ maps or their averages $\langle Wr^{(s)}(i,s)\rangle$ with the preformed hooked (left) or free (right) juxtaposition placed at the center. In (a), the $Wr^{(s)}(i,s)$ map on the left is for the $n = 14$ conformation in Fig. 11(a), whereas the $Wr^{(s)}(i,s)$ map on the right is for the $n = 18$ conformation in Fig. 11(b). The average $\langle Wr^{(s)}(i,s)\rangle$ maps in (b) and (c) are, respectively, for chain lengths $n = 32$ and $n = 50$. Torsional energy was not used in the computation of these $\langle Wr^{(s)}(i,s)\rangle$ maps.